IIETA International Information and Engineering Technology Association
Advancing the World of Information and Engineering

Mathematical Modelling of Engineering Problems
Vol. 12, No. 7, July, 2025, pp. 2263-2270
Journal homepage: http://iieta.org/journals/mmep

Interference Avoiding Among QAM-MIMO Signals Transceiver Performance Based Bands Sharing

Emad Hmood Salman[1*], Montadar Abas Taher[1], Haidar N. Al-Anbagi[1], Yousif I. Hammadi[2]

[1] Department of Communications Engineering, College of Engineering, University of Diyala, Baquba 32001, Iraq
[2] Department of Medical Instruments Engineering Techniques, Bilad Alrafidain University College, Baquba 32001, Iraq

Corresponding Author Email: emad_salman_eng@uodiyala.edu.iq

https://doi.org/10.18280/mmep.120707

Received: 4 July 2024
Revised: 13 October 2024
Accepted: 20 October 2024
Available online: 31 July 2025

Keywords:
5G signal, interference, MIMO, QAM, radar, Rayleigh fading channel

ABSTRACT

In contemporary communication systems such as 5G and next-generation cellular networks, the MIMO approach is crucial. Large-scale data transmission is a well-known feature of these sophisticated systems. In cellular systems, it is imperative to reduce the interference that QAM-MIMO signals produced between the transmitter and the receiver. This article examines the interference performance of QAM-MIMO transmissions. The number of transmitter antennas, number of reception antennas, number of sub-arrays, the Rayleigh fading channel, and the target direction are among the key variables affecting how the proposed model operates. To identify signal interference, we find and examine the side lobes and beamforming. Furthermore, considering the gap between wavelengths leads to benefits from the QAM-MIMO approach. The numerical and graphical results demonstrate how 5G transmissions interfered with prior settings. Furthermore, a comparison of the proposed model with similar research is also achieved. The outcomes demonstrated that the interference characteristics were analyzed by the proposed model.

1. INTRODUCTION

5G and other wireless technologies increase data transfer rates in constrained frequency ranges, however problems with broadband proliferation and ineffective resource distribution result in underutilized band and difficulties for cellular network operators. To solve these issues, more research is required on band sharing between public and private networks, including radars [1-4].

While band coexistence presents a viable way to use various frequency bands, 5G and radar equipment can cause interference. One of the main priorities should be controlling overlapping electromagnetic waves, especially those from radars. Band sharing does have certain disadvantages, too, like the requirement to shield incumbents from cellular system interference in common frequency regions. Furthermore, communication systems near radar systems cannot function properly due to the tremendous transmit power of radars overwhelming receiver amplifiers [5-7].

Full-duplex communication systems allow simultaneous data transmission and reception in the time and frequency domains, which maximizes the utilization of available band. With full-duplex technology, as opposed to passive band sharing, government organizations can use available radar frequencies or stay out of exclusion zones while still protecting themselves from disturbance. By increasing band availability and enhancing service quality, this approach opens the door for later band sharing projects including government users and cutting-edge technologies [8-10].

There are a number of proactive approaches in the literature that deal with interference caused by band sharing. Utilizing the diversity of waveforms is the key concept in many of the MIMO radar techniques that have been developed. Two primary types of MIMO radars can be distinguished based on the array configurations that are employed. In order to capture the spatial diversity of the target's radar cross section, the first type uses widely separated transmit/receive antennas. The second form of MIMO radar focuses on cohering a beam towards a certain direction in space by using arrays of closely spaced transmit/receive antennas. The relevant current research is discussed in the following. On the perspective of MIMO joint radar-communication systems, some of related works are described below. The authors investigated orthogonal frequency division multiplexing, orthogonal chirp division multiplexing, phase-modulated continuous wave, and sequence of chirps for a hybrid radar-communication system in 2021 [11]. The study reveals phase-modulated continuous-wave and sequence chirp modulation schemes are suitable for low data rate applications, including front-end overlap in integrated radar-communication systems, and necessitate multiplexing to prevent dynamic range decline. A thorough analysis of cooperative communication and radar systems was carried out [12]. The text is divided into three sections: communication, radar, and integrated communication and radar, emphasizing the need to consider millimeter wave and frequency-hopping signals for high data rates. In 2023, Nguyen et al. [13] have studied an effective joint radar-communications design that incorporates a MIMO-subcarrier

allocation method. This method reduces the beam-forming's degrees of freedom and significantly degrades communication performance, particularly when there are stringent radar recognition limitations. In order to solve this, communications are given their own dedicated subcarriers, which remove interference from the radar function while maintaining strict design limitations to guarantee the radar's recognition accuracy. Current year, by combining radar and communications systems, Ozkaptan et al. [14] have proposed the mmWave to address the transmission band between vehicles and everything. Using the same waveform and technology for both operations, this approach proved to be a comprehensive way to use these bands. An OFDM-MIMO signal operating in the 24 GHz mmWave range was being tested. Despite being built on the MUSIC algorithm, the suggested system resulted in a significant level of computing complexity. Because of the enhanced radar processing capabilities made possible by the completely digital MIMO design, the findings have improved. On the other hand, the viewpoint of beam-forming system has been processed through radar-communication system too. A well-optimized time and band allocation technique for coexistence networks of distributed radar–communication is put out by Zhang et al. [15]. Subject to limitations on dwell time and band utilization, the system is built to minimize the sum of weighted position Bayesian Cramér-Rao lower bounds while meeting communication downlink needs. Simulations show that in terms of tracking performance, the suggested strategy performs better than two baseline allocation strategies. A performance analysis of the trade-off between MU-MIMO and MIMO communication systems is provided by Chen et al. [16]. The study utilized weighted mean square error and sequential convex approximation techniques to determine the optimal border region for communication and radar foci, and expanded the study to create a simpler level of beam-forming for channel selection and zero-forcing scenarios. He et al. [17] propose a modal using the penalty dual decomposition technique to address radar transmitting power issues in both low-power and high-power settings. They also create a beam-forming system using block coordinate descent to prevent interference and reduce complexity using a non-convex objective function.

In this paper, a performance model for preventing interference between 5G communications systems and radar is suggested. Both 5G and radar communication systems use many antennas on both the transmitter and the receiver in accordance with the MIMO principle using QAM signal. The proposed model will prohibit the interference that may occur through a channel with Rayleigh fading kid between communications system and radar-based MIMO-5G technique. Additionally, it is also damped the weakness in the MIMO-radar performance. The suggested model is also used to MIMO sub-arrays in order to investigate the interference that occurs between MIMO radar and regular QAM signals. The contributions of the proposed model can be summarized as follows:

- The proposed model eliminates the side-lobe carefully then the interference will be decreased.
- The band sharing of focusing radar is efficient since the channel among the 5G communication systems has a nullified-space.
- The coexistence between communications and radar systems has been enhanced due to the overlapping of MIMO radar.

The rest of this paper is organized as follows. Section II describes the fundamentals of sharing of bands through the MIMO. Section III introduces the proposed avoiding-overlapping MIMO radar system. Section IV discusses and analyses the results of simulation running and offers details with benchmarks. Last Section V determines the article with suggestion of future works.

2. BACKGROUND OF MIMO CONCEPT BASED BANDS SHARING

The Federal Communications Commission (FCC) has granted permission for the commercial use of specific frequency ranges for transmission, allowing radar, satellite, and communication systems to coexist. This change has led to the development of methods to expand the capacity of these systems, reduce interference, and optimize shared usage, all of which are made possible by the application of the MIMO concept [18-20].

Radar and communication are not given priority in these systems; instead, both are integrated and optimized from the start. These systems offer a flexible balance between the two roles that can be adjusted in accordance with the demands of a given application. This method allows for more design freedom because it is not limited by existing communication or radar systems. To gain a deeper understanding of the joint design of communication and radar systems, it is important to first compare them, highlighting their similarities and differences. Below is a comparison of the two functions based on signal waveforms, transmission power, bandwidth, and other key specifications [21].

• Signal Waveforms: Broad bandwidth, unmodulated single-carrier pulsed or continuous-wave signals are used in radar waveforms, which are generally basic and intended for sharp and narrow ambiguity functions. On the other hand, communication signals can be discontinuous in space, time, and frequency. They can have more intricate structures with sophisticated modulations that combine both unmodulated (training or pilot) and modulated data symbols.

• Transmitter Power: While short-term continuous-wave radars require less power, long-range pulsed radars usually demand considerable transmission power. Since communication systems have a smaller coverage area, they often use less power to function. In order to facilitate effective power amplification for long-range performance, radar signals are engineered to have a low peak-to-average power ratio.

• Bandwidth: While continuous-wave radars send continuous waveforms across a wide frequency range, such as chirp signals, pulsed radars transmit short, wide-bandwidth pulses followed by silent intervals to detect target echoes. Large bandwidth is needed by radars in order to improve range resolution. Radar waveforms are very different from the much smaller, bandwidth-restricted signals used by communication systems.

• Frequency of Operation: Radars operate in the L, S, C, X, Ku, K, and Ka band operational frequency bands. W band frequency is used by automotive radars. Communication frequencies are found in the mmWave and sub-6 GHz regions. For 6G, terahertz frequencies are being used.

• Clock Synchronization: To prevent uncertainty in the calculation of recognizing characteristics, radars synchronize the clocks of their transmitter and receiver. Colocated nodes may share a clock in the context of communications, whereas non-colocated nodes typically do not.

• Performance Metrics: Metrics like peak-to-sidelobe level ratio, signal-to-clutter ratio, maximum range and velocity, and resolution in terms of range, Doppler, and angle are used to assess radar performance. On the other hand, bit error rate, capacity, latency, throughput, outage possibility, and signal-to-interference-plus-noise ratio are used to evaluate wireless communication systems.

The 5G-MIMO communication and radar antenna systems work together and are set up in a similar way. Due to the many kinds of channel reactions that might arise when signals are being sent, let $\boldsymbol{y}_{chan}(t)$ symbolize the signal that is sent through these channels. This can be expressed as follows:

$$\boldsymbol{y}_{chan}(t) = \boldsymbol{H}_{int}^{C_{rx}\times R_{tx}}\boldsymbol{x}_{rad}(t) + \boldsymbol{H}^{C_{rx}\times C_{tx}}\boldsymbol{x}_{com}(t) \quad (1)$$

Thus, the signal, $\boldsymbol{y}_{com}(t)$, that are received by the communications system is represented by:

$$\boldsymbol{y}_{com}(t) = \boldsymbol{y}_{chan}(t) + \boldsymbol{n}_{Ray}(t) \quad (2)$$

where, $\boldsymbol{x}_{rad}(t)$ and $\boldsymbol{x}_{com}(t)$ denote the transmitted radar and transmitted communications signals, respectively. $\boldsymbol{H}_{int}$ and $\boldsymbol{H}$ denote the interference channel radar versus communications systems and channel that is used by the communications system, respectively. In addition, C_{rx}, C_{tx}, R_{rx}, and R_{tx} represent communications receiver antennas number, communications transmitter antennas number, radar receiver antennas number, and radar transmitter antennas number, respectively. $\boldsymbol{n}_{Ray}(t)$ denotes the Rayleigh fading channel noise.

Communication and radar systems operate in a cooperative environment, efficiently collaborating and exchanging data, ensuring each system prevents disturbances to the others [22].

The study explores a radar-centered design process, aiming to retrieve interference channel status information from the radar terminal. The MIMO radar's objective is to generate distinct waveforms to prevent network interference, with an example of coexistence shown in Figure 1.

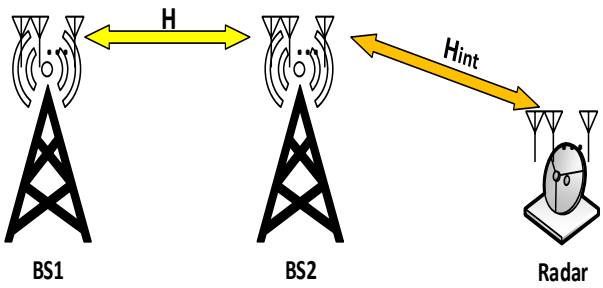

Figure 1. The MIMO of 5G communications and radar systems

This study defines the fundamental elements of a structured MIMO radar configuration, suggesting that transmitting and receiving antennas should be close to each other.

The transmitted radar signal, $\boldsymbol{x}_{rad}(t)$, can be extracted into time-domain $x(t)$ and transmitted-guided waveform $x_{gui}(\theta)$ notations as follows:

$$\begin{aligned}\boldsymbol{x}_{rad}(t) &= [x_1(t)x_2(t)\dots x_{M_T}(t)] \\ &= [x_{gui1}(\theta)\phi_1(t)x_{gui2}(\theta)\phi_2(t)\dots x_{guiM_T}(\theta)\phi_{M_T}(t)]\end{aligned} \quad (3)$$

It is well acknowledged that the whole transmitted waveform obeys the orthogonality principle and that each component is mutually perpendicular to the others [23].

$$\boldsymbol{x}_{rad}(t) = \boldsymbol{x}_{gui}(\theta)\odot\phi(t) \quad (4)$$

where, Θ is an N-ary dot operator.

On the other hand, the transmitted-guided waveform can be represented as follows

$$\begin{aligned}\boldsymbol{x}_{gui}(\theta) &= [x_{gui1}(\theta)x_{gui2}(\theta)\dots x_{guiM_T}(\theta)] \\ &= [1e^{-j2\pi d_T\sin\theta}\dots e^{-j2\pi d_T(M_T-1)\sin\theta}]\end{aligned} \quad (5)$$

Under Rayleigh fading channel, $\boldsymbol{y}_{rad}(t)$ represents the received radar signal, which can be stated as

$$\boldsymbol{y}_{rad}(t) = \boldsymbol{y}_t(t) + \boldsymbol{y}_{jam}(t) + \boldsymbol{n}_{Ray}(t) \quad (6)$$

where, $\boldsymbol{y}_{jam}(t)$ denotes a jamming signal. In addition, $\boldsymbol{y}_t(t)$ denotes a target signal and it can be formulated as follows

$$\boldsymbol{y}_t(t) = \beta_s\left(\boldsymbol{x}_{gui}(\theta_s)\varphi(t)\right)\boldsymbol{y}_{gui}(\theta_s) \quad (7)$$

here, θ_s, β_s, and $\boldsymbol{y}_{gui}(\theta)$ denote the target direction, the complex reflection coefficient, and the receive steering vector for the direction θ and $M_R \times 1$, respectively. In addition, $\boldsymbol{y}_{gui}(\theta)$ can be stated as

$$\begin{aligned}\boldsymbol{y}_{gui}(\theta) &= [y_{gui1}(\theta)y_{gui2}(\theta)\dots y_{guiM_R}(\theta)] \\ &= [1e^{-j2\pi d_R\sin\theta}\dots e^{-j2\pi d_R(M_R-1)\sin\theta}]\end{aligned} \quad (8)$$

3. PROPOSED AVOIDING-OVERLAPPED MIMO-RADAR BASED BANDS SHARING

The unique needs of both tasks should be the main-focus of system design and optimization in order to create a reasonable compromise between radar and communication performance. The joint optimal waveform design presents the main challenge. Phased array, fully-digital MIMO, and hybrid array architectures are the three types of hardware for such systems. They employ analog, digital, and hybrid analog-digital beam-forming, respectively, as their respective beam-forming methodologies.

- Analog beam-forming: Phase shifters are used to feed a single signal to every antenna, directing it in a certain direction. It is straightforward, economical, power-efficient; however, it can only produce a single beam, and in wideband transmissions, it exhibits beam squint.
- Digital beam-forming: Similar to MIMO systems, each antenna has its own RF chain and uses spatial pre-coding to create signals in the digital baseband. Although this method is more complicated, costly, and power-intensive, it supports multiple beams and wideband operation.
- Hybrid beam-forming: Creates sub-arrays within of a larger array and uses analog beam-forming within each sub-array. This technique combines elements of both analog and digital beam-forming. It lessens the drawbacks of both pure analog and digital methods by providing a performance balance.

It is possible to construct performance criteria for communication and radar systems separately or as a weighted composite function. Mutual information is the greatest amount of data that can be transferred between a source and a receiver

in a communication system. For radars, it measures the quantity of information gained from the received signal about the environment. Optimizing the radar-communication waveform using a benchmark signal with a desirable beam-pattern—typically a well-known radar waveform with low side-lobe levels and strong correlation—is another method of design. In order to ensure that the waveform maintains a beam-pattern identical to the radar's while meeting communication needs this reduces the impact of communication data and channel randomness. Minimizing the mean-square estimation error for important parameters like range, angle, and velocity is the key to accurate finding in radar systems. The Cramér-Rao Lower Bound is a crucial performance metric that establishes the lower bound for mean-square estimation error. To maximize identifying accuracy, Cramér-Rao Lower Bound must be taken into account in the collaborative design of communication-radar waveforms since it is impacted by transmitted waveforms.

To introduce the proposed system with details, this section is divided into two following sub-section as shown below:

3.1 MIMO-radar avoiding-overlapped formulation

A novel antenna design based-MIMO is presented in current sub-section, it is also known as overlap-MIMO, which allows beam-forming for both transmit and receive arrays by splitting every array into many overlapped sub-arrays. A fundamental idea is fragmenting the transmitted arrays into many sub-arrays, i.e., K, allowing for overlap [24].

At the kth sub-array's output, the signal complex envelope is represented as

$$s_k = \sqrt{\frac{M_T}{K}}\phi_k(t) \odot w_k, \quad k = 1, \dots, K \quad \text{and } 1 \le K \le M_T \tag{9}$$

where, the vectors of $M_m \times 1$ includes ϕ_k and w_k. The last vector contains both real and imaginary components with a unit-norm that contains M_m beam-forming weights. M_m orthogonal waveforms make up the waveform vector that is the former. It is noteworthy that M_m denotes the quantity of antenna elements present in every sub-array. M_m is defined as M_T–K+1.

The transmitted signal, $\phi(t)_k^m$, can be formulated as follows for every orthogonal waveform,

$$\phi_k^m = Q(t)e^{j2\pi(mk/T_0)t} \tag{10}$$

where, the pulse shape is represented by $Q(t)$ for duration T_0, $m = 1, \dots, M_m$ and $k = 1, \dots, K$ [25].

When a target is placed in the far field at angle θ, the signal that is reflected off it is described as:

$$r(t,\theta) = \sqrt{\frac{M_T}{K}}\beta(\theta)\sum_{k=1}^{K}\sum_{m=1}^{M_m} w_k^m \phi_k^m(t) d_k^m(\theta) \tag{11}$$

where, $\beta(\theta)$ is the coefficient of reflection, and $d_k^m(\theta)$ is the vector of waveform diversity that is defined as $e^{-j\tau_k^m(\theta)}$. In addition, the necessary time, $\tau_k^m(\theta)$, for the wave to travel from the first component to the next component.

It is possible to express the complex vector that was received from the array observation as

$$y_{Radar}(t) = r(t,\theta_s)b(\theta_s) + \sum_{i}^{\varepsilon} r(t,\theta_i)b(\theta_i) + n_{Ray}(t) \tag{12}$$

where, ε is the interfering signals number, $b(\theta)$ is the vector of receive steering with size $M_R \times 1$ associated with angle θ, and $n_{Ray}(t)$ is a Rayleigh-fading channel noise.

A vector of essential data may generate as $[1 \times M_R K M_m]^{\mathrm{T}}$, by filtering with matched-filter $y_{Radar}(t)$ for every waveform that is noted with $\{\phi_k^m\}_{m=1,k=1}^{M_m,K}$.

$$y_v = \sqrt{\frac{M_T}{K}}\beta_s u(\theta_s) + \sum_{i}^{\varepsilon}\sqrt{\frac{M_T}{K}}\beta_i u(\theta_i) + n_{Ray}(t) \tag{13}$$

$$u(\theta) = (c(\theta) \odot d(\theta)) \otimes b(\theta) \tag{14}$$

Eq. (14) represents a vector of virtual steering with $[1 \times M_R K M_m]^{\mathrm{T}}$, a middle vector $c = \{w_k^m a_k^m\}_{m=1,k=1}^{M_m,K}$ of size $[1 \times M_m K]^{\mathrm{T}}$, and vector of waveforms diversity $d = \left\{e^{-j\tau_k^m(\theta)}\right\}_{m=1,k=1}^{M_m,K}$ of size $M_m K \times 1$ [26].

The beam-former weight vectors for the kth transmitting sub-array in non-adaptive beam-forming are given as.

$$w_k = \frac{a_k(\theta_s)}{\|a_k(\theta_s)\|} = \frac{a_k(\theta_s)}{\sqrt{M_T - K + 1}}, \quad k = 1, \dots, K \tag{15}$$

Such vectors are given for the receiving sub-arrays as $w_d = (c(\theta_s) \odot d(\theta_s)) \otimes b(\theta_s)$.

Let $Norm(\theta)$ be the normalized overall beam-pattern.

$$Norm(\theta) = \frac{|w_d^H u(\theta)|^2}{|w_d^H u(\theta_s)|^2} = \frac{|u^H(\theta_s)u(\theta)|^2}{\|u(\theta_s)\|^4} \tag{16}$$

$a_1^H a_1(\theta_s) = \cdots a_K^H a_K(\theta_s)$ is obtained specifically for the situation of a uniform linear array. For a uniform linear array with K overlapped transmit sub-arrays, the beam pattern of the overlapped-MIMO radar can be stated as follows using Eq. (16):

$$Norm_K(\theta) = \frac{|a_K^H(\theta_s)a_K(\theta)[(d(\theta_s) \otimes b(\theta_s))^H (d(\theta) \otimes b(\theta))]|^2}{\|a_K^H(\theta_s)\|^4 \|d(\theta_s) \otimes b(\theta_s)\|^4} \tag{17}$$

3.2 Sharing of bands based on MIMO-radar system

This subsection details a radar projection algorithm-based band-sharing technique, utilizing a projection approach of null space [27], the approach projected the signal of overlap-MIMO radar on a communication interference channel's null space, requiring prior channel side information that can be obtained and shared with the radar system [28].

The suggested technique works like this: the radar first gathers **H**, the channel side data that connects the radar to the communication channels. The available number of null space that are for projection will be calculated, and it equals M_T–N_R. Next, it determines the projection of the channel matrix, **P**, then produces a fresh signal of radar, $\hat{x}_{Radar}$. In order to prevent radar interference, the overlapped-MIMO radar waveform projected onto **H**'s null space can be written as follows: where **H** demonstrates the channel matrix.

$$\hat{x}_{Radar}(t) = \boldsymbol{P}x_{Radar}(t) \quad (18)$$

4. RESULTS OF SIMULATION

In this section, the results are obtained and analyzed with many parameters that are used in the construction of the proposed system. The obtained results of the proposed system have been offered by using the MATLAB software to simulate the 5G signal based MIMO technique. The 5G signal is implemented according to F-OFDM-MIMO technique and modulated with QAM modulation. The F-OFDM signal is generated with the following characteristics to fulfill the 5G communication systems requirement as shown in the Table 1.

Table 1. F-OFDM-MIMO signal characteristics based 5G communications system

Number of TX (Radar) antenna = 30
Number of RX antenna = 30
Number of FFT = 1024
Number of Resource Block = 50
Number of sub-carriers = 12
Length of cyclic-prefix = 72
Bits/Sub-carrier = 6
Tone off-set = 2.5
Length of filter = 513
64 QAM

In this simulation, the adjacent element of antennas is halved the wavelength separately because in both cases the element spacing is 0.5. The signal experiences Rayleigh-Noise distribution when it moves through a Rayleigh fading channel. Every component of the antenna is omnidirectional. In addition, the sub-arrays are divided into six ratios as shown in the following figures.

The general beam-pattern for six distinct MIMO radar designs is shown in Figure 2: There are six types of overlapped MIMO radars:

(1) radar with $K = 5$ (indicating five sub-array),
(2) radar with $K = 10$,
(3) radar with $K = 15$,
(4) radar with $K = 20$,
(5) radar with $K = 25$,
(6) MIMO radar (pure MIMO) with $K = 30$.

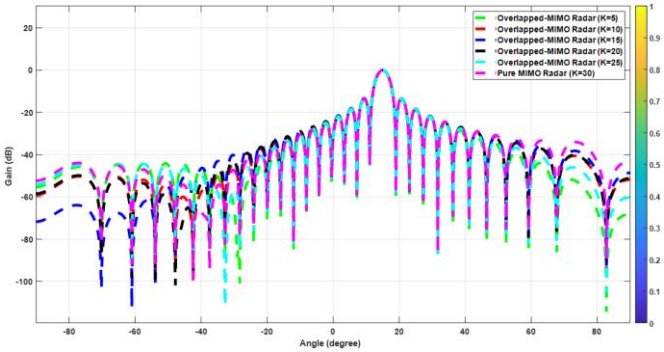

Figure 2. Total beam-pattern using conventional transmit-receive beam-former

The overlapping-MIMO radars in this context come in two orientations: 10 overlapped sub-arrays with 21 antenna elements each, 15 overlapped sub-arrays with 16 antenna elements each, and 20 overlapped sub-arrays with 11 antenna elements each. The overall transmit/receive beam-patterns of the pure MIMO-radar, $K = 30$, the overlap-MIMO radar, $K = 5$, and the overlap-MIMO radar, $K = 25$ are found to be approximately similar. On the other hand, the overlapped-MIMO radar exhibits notably superior side-lobe suppression when juxtaposed with the pure MIMO radar's beam-pattern.

Six distinct MIMO radar configurations using the null space projection algorithm are shown in Figure 3's overall beam-pattern. Null Space Projection is denoted by NSP. First, overlap-MIMO radar for ($K = 5$) addition to null space projection (signaling five sub-array). Second, overlap-MIMO radar for ($K = 10$) addition to null space projection. Third, overlap-MIMO radar for ($K = 15$) addition to null space projection. Forth, overlap-MIMO radar for ($K = 20$) addition to null space projection. Fifth, overlap-MIMO radar for ($K = 25$) addition to null space projection. Finally, radar-MIMO for ($K = 30$) addition to null space projection, only MIMO. As anticipated, it is found that the projection approaches have lessened side-lobe elimination. It still offers superior suppression, nevertheless, as compared to radar-MIMO alone. The major benefit is on the communication system side, where coexistence is made possible by the null space projection algorithm's reduction of radar interference with the communication system.

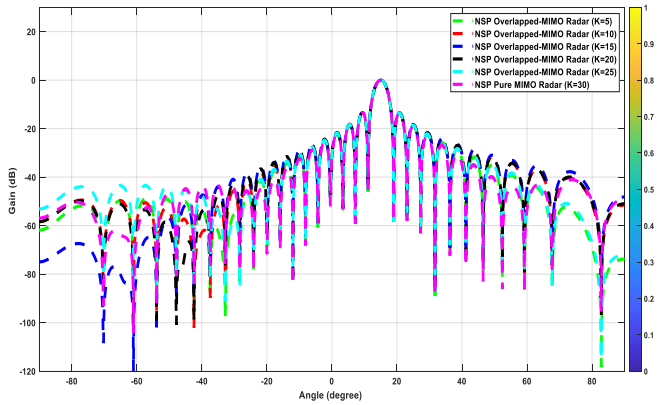

Figure 3. Total beam-pattern using conventional transmit/receive beam-former and null space projection

Figures 2 and 3 depicted the overall beam patterns for the conventional transmit-receive beam-former and the overlapped sub-array design, respectively, using 30 antenna components, to evaluate the advantages of utilizing virtual sub-arrays. Because both phased-array and MIMO radars essentially use the same number of transmitting arrays, the results showed that their overall transmit and receive beam-patterns was comparable. On the other hand, the overlapping MIMO radar's beam-pattern is noticeably better than that of the phased-array and conventional MIMO radars, which is helpful for target uncovering. The beam-patterns of all radar systems with null-space projection applied are also shown in the figures. The overlapping MIMO radar nevertheless provides better suppression than the other two radars, even though null-space projection lessens side-lobe suppression. Moreover, null-space projection minimizes radar system interference to the communication system, allowing for band sharing.

On the other hand, the surface plot in Figure 4 depicts the total gain of beam-pattern vs. number of sub-arrays vs. angle of direction for the 64-QAM scenario. It can be seen that the biggest gain is little bit lower than 0 dB with 15 degree angle

direction and more than or equal to 10 sub-arrays. Furthermore, once the angle increases or decreases, the gain become worse and decreasing significantly.

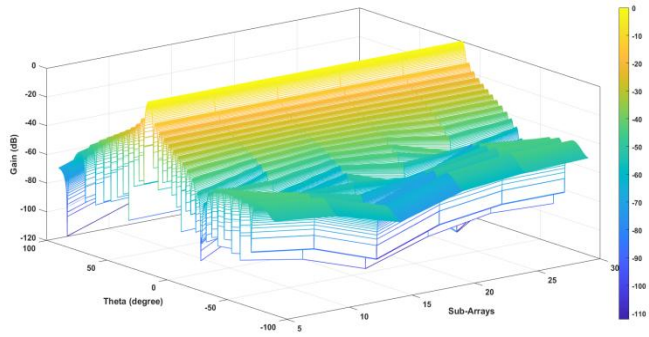

Figure 4. Total beam-pattern gain vs. number of sub-arrays vs. angle of direction

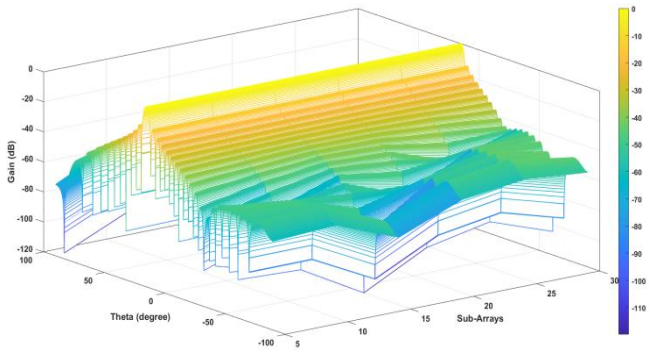

Figure 5. Total beam-pattern gain with null space projection vs. number of sub-arrays vs. angle of direction

As in Figure 4, Figure 5 is a surface plot and shows the total gain of beam-pattern with null space projection vs. number of sub-arrays vs. angle of direction for the 64-QAM scenario. It can be seen that the gain is decreased along with increasing or decreasing the angle of direction for greater or lower than 15 degrees. However, the biggest gain is obtained when the number of sub-arrays greater than or equal to seven. In addition, the number of sub-arrays can be considered to be a crucial factor since it improves the total gain.

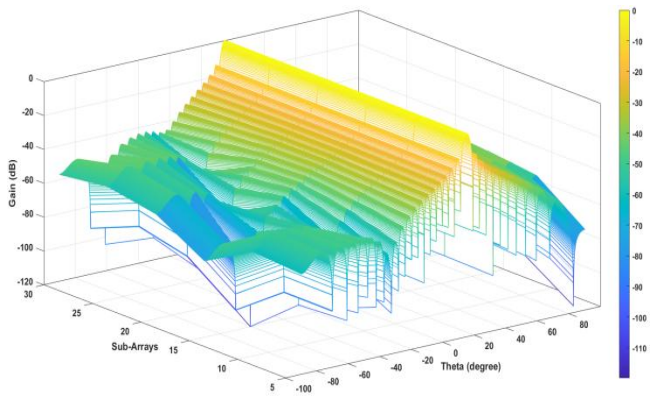

Figure 6. Total beam-pattern gain with null space projection vs. angle of direction vs. number of sub-arrays

Figure 6 is the same surface plot as Figure 5 with a direction (angle) perspective. It also shows the total gain of beam-pattern with null space projection vs. number of sub-arrays vs. angle of direction for the 64-QAM scenario. It can be seen that the side-lobes are vanished once the angle greater than or lower than 30 degree. In addition, the gain is decreased along with the vanishing side-lobes.

All in all, once the channel noise is spread in accordance with the Rayleigh fading channel, the suggested system improves the prohibition, as shown by the prior figures and surfaces. Furthermore, a larger number of antennas are used to test the suggested system's complexity. However, the test signal mimics the real-world situation by using a 5G communication system signal. The earlier comparable works that are listed in the first section as a literature survey did not accomplish any of the earlier milestones or contributions. The related works did not study their systems with Rayleigh fading noise kind whereas the proposed system has been applied on it. In addition, the findings of the proposed system are better than those related works although the related works had been applied only on AWGN.

5. CONCLUSIONS

This paper presents an overlapped-MIMO antenna design and the null space projection band-sharing technique to allow coexistence of communication systems and radars. In the presence of Rayleigh fading channel noise, the system evaluates the MIMO concept based on 5G signals. The radar's transmit array in the overlapped-MIMO design is split up into many overlapping sub-arrays, each of which sends signals orthogonal to those of the other sub-arrays and to each other. Comparing this architecture to traditional MIMO radar, it improves side-lobe suppression, boosts diversity gain, and expands the effective transmit array size, all of which make it more compatible with communication systems. It is advised that this system be investigated further in the context of 6G, whether or not NOMA integration is present.

REFERENCES

[1] Li, Z., Pan, J., Hu, H., Zhu, H. (2022). Recent advances in new materials for 6G communications. Advanced Electronic Materials, 8(3): 2100978. https://doi.org/10.1002/aelm.202100978

[2] Sabat, D., Pattanayak, P., Kumar, A., Prasad, G. (2023). A contemporary review on user scheduling techniques and feedback reduction strategies towards the development of 5G and beyond communications. Physical Communication, 58: 102070. https://doi.org/10.1016/j.phycom.2023.102070

[3] Lehr, W. (2020). Economics of spectrum sharing, valuation, and secondary markets. Spectrum Sharing: The Next Frontier in Wireless Networks, pp. 361-388. https://doi.org/10.1002/9781119551539.ch18

[4] Sathya, V., Kala, S.M., Naidu, K. (2023). Heterogenous networks: From small cells to 5G NR-U. Wireless Personal Communications, 128(4): 2779-2810. https://doi.org/10.1007/s11277-022-10070-z

[5] Parvini, M., Zarif, A.H., Nouruzi, A., Mokari, N., Javan, M.R., Abbasi, B., Yanikomeroglu, H. (2022). A comprehensive survey of spectrum sharing schemes from a standardization and implementation perspective. arXiv preprint arXiv:2203.11125. https://doi.org/10.48550/arXiv.2203.11125

[6] Casetti, C. (2023). Get yourself a private, portable 5G network [Mobile Radio]. IEEE Vehicular Technology Magazine, 18(2): 9-15. https://doi.org/10.1109/MVT.2023.3263073

[7] Parvini, M., Zarif, A.H., Nouruzi, A., Mokari, N., Javan, M.R., et al. (2023). Spectrum sharing schemes from 4G to 5G and beyond: Protocol flow, regulation, ecosystem, economic. IEEE Open Journal of the Communications Society, 4: 464-517. https://doi.org/10.1109/OJCOMS.2023.3238569

[8] Xiao, Z., Zeng, Y. (2022). Waveform design and performance analysis for full-duplex integrated sensing and communication. IEEE Journal on Selected Areas in Communications, 40(6): 1823-1837. https://doi.org/10.1109/JSAC.2022.3155509

[9] Kassri, N., Ennouaary, A., Bah, S., Baghdadi, H. (2021). A review on SDR, spectrum sensing, and CR-based IoT in cognitive radio networks. International Journal of Advanced Computer Science and Applications, 12(6): 100-121. https://doi.org/10.14569/IJACSA.2021.0120613

[10] Kulin, M., Kazaz, T., De Poorter, E., Moerman, I. (2021). A survey on machine learning-based performance improvement of wireless networks: PHY, MAC and network layer. Electronics, 10(3): 318. https://doi.org/10.3390/electronics10030318

[11] De Oliveira, L.G., Nuss, B., Alabd, M.B., Diewald, A., Pauli, M., Zwick, T. (2021). Joint radar-communication systems: Modulation schemes and system design. IEEE Transactions on Microwave Theory and Techniques, 70(3): 1521-1551. https://doi.org/10.1109/TMTT.2021.3126887

[12] Zhang, J.A., Liu, F., Masouros, C., Heath, R.W., Feng, Z., Zheng, L., Petropulu, A. (2021). An overview of signal processing techniques for joint communication and radar sensing. IEEE Journal of Selected Topics in Signal Processing, 15(6): 1295-1315. https://doi.org/10.1109/JSTSP.2021.3113120

[13] Nguyen, N.T., Shlezinger, N., Eldar, Y.C., Juntti, M. (2023). Multiuser MIMO wideband joint communications and sensing system with subcarrier allocation. IEEE Transactions on Signal Processing, 71: 2997-3013. https://doi.org/10.1109/TSP.2023.3302622

[14] Ozkaptan, C.D., Zhu, H., Ekici, E., Altintas, O. (2023). A mmWave MIMO joint radar-communication testbed with radar-assisted precoding. IEEE Transactions on Wireless Communications, 23(7): 7079-7094. https://doi.org/10.1109/TWC.2023.3337282

[15] Zhang, H., Liu, W., Liu, Y., Zhang, Q., Liu, B. (2023). Joint target and user assignment as well as dwell time and spectrum allocation in a distributed radar–communication coexistence network. IEEE Transactions on Aerospace and Electronic Systems, 60(1): 1159-1175. https://doi.org/10.1109/TAES.2023.3335179

[16] Chen, L., Wang, Z., Du, Y., Chen, Y., Yu, F.R. (2022). Generalized transceiver beamforming for DFRC with MIMO radar and MU-MIMO communication. IEEE Journal on Selected Areas in Communications, 40(6): 1795-1808. https://doi.org/10.1109/JSAC.2022.3155515

[17] He, Y., Cai, Y., Mao, H., Yu, G. (2022). RIS-assisted communication radar coexistence: Joint beamforming design and analysis. IEEE Journal on Selected Areas in Communications, 40(7): 2131-2145. https://doi.org/10.1109/JSAC.2022.3155507

[18] Qian, J., Zhao, L., Shi, X., Fu, N., Wang, S. (2022). Cooperative design for MIMO radar-communication spectral sharing system based on mutual information optimization. IEEE Sensors Journal, 22(17): 17184-17193. https://doi.org/10.1109/JSEN.2022.3192348

[19] Villa, D., Uvaydov, D., Bonati, L., Johari, P., Jornet, J.M., Melodia, T. (2023). Twinning commercial radio waveforms in the colosseum wireless network emulator. In Proceedings of the 17th ACM Workshop on Wireless Network Testbeds, Experimental Evaluation & Characterization, Madrid, Spain, pp. 33-40. https://doi.org/10.1145/3615453.3616519

[20] Lialios, D.I., Zekios, C.L., Georgakopoulos, S.V., Kyriacou, G.A. (2022). A novel RF to millimeter waves frequency translation scheme for ultra-wideband beamformers supporting the Sub-6 GHz band. IEEE Transactions on Antennas and Propagation, 70(12): 11718-11733. https://doi.org/10.1109/TAP.2022.3210698

[21] Hanif, A., Ahmed, S., Alouini, M.S., Al-Naffouri, T.Y. (2025). Exploring the synergy: A review of dual-functional radar communication systems. IEEE Aerospace and Electronic Systems Magazine, 2025: 1-26. https://doi.org/10.1109/MAES.2025.3551690

[22] Zhang, J.A., Liu, F., Masouros, C., Heath, R.W., Feng, Z., Zheng, L., Petropulu, A. (2021). An overview of signal processing techniques for joint communication and radar sensing. IEEE Journal of Selected Topics in Signal Processing, 15(6): 1295-1315. https://doi.org/10.1109/JSTSP.2021.3113120

[23] Lu, J., Yang, J., Hou, B., Zhu, F., Liu, G. (2021). Covariance matrix reconstruction and steering vector estimation for robust adaptive transmit/receive beamforming in full phased-MIMO radar. Electronics Letters, 57(7): 288-291. https://doi.org/10.1049/ell2.12120

[24] Ranjith, S., Jayarin, P.J., Sekar, A.C. (2023). A multi-fusion integrated end-to-end deep kernel CNN based channel estimation for hybrid range UM-MIMO 6G communication systems. Applied Acoustics, 210: 109427. https://doi.org/10.1016/j.apacoust.2023.109427

[25] Sun, S., Hu, Y., Mishra, K.V., Petropulu, A.P. (2024). Widely separated MIMO radar using matrix completion. IEEE Transactions on Radar Systems, 2: 180-196. https://doi.org/10.1109/TRS.2024.3362693

[26] Xiong, Y., Xie, W., Wang, Y. (2023). Space time adaptive processing for airborne MIMO radar based on space time sampling matrix. Signal Processing, 211: 109119. https://doi.org/10.1016/j.sigpro.2023.109119

[27] Tolley, J., Makin, C., Dietrich, C.B. (2023). Systematization of knowledge: Spectrum sharing between radar and communications. IEEE Access, 11: 138347-138374. https://doi.org/10.1109/ACCESS.2023.3339579

[28] Zhang, H., Chen, L., Han, K., Chen, Y., Wei, G. (2023). Coexistence designs of radar and communication systems in a multi-path scenario. IEEE Transactions on Vehicular Technology, 73(3): 3733-3749. https://doi.org/10.1109/TVT.2023.3325544

NOMENCLATURE

5G	Fifth Generation
MIMO	Multi-Input-Multi-Output
QAM	Quadrature Amplitude Modulation
QoS	Quality of Service
SINR	Signal Interference Noise Ratio
FCC	Federal Communications Commission
$\mathbf{y}_{chan}(t)$	The signal of channel
$\mathbf{y}_{com}(t)$	The received signal
$\mathbf{n}_{Ray}(t)$	Rayleigh fading channel noise
$\mathbf{x}_{rad}(t)$	Transmitted radar signal
$\mathbf{x}_{com}(t)$	Transmitted communications signal
$\mathbf{H}_{int}$	The interference channel radar versus communications systems
$\mathbf{H}$	The channel that is used by the communications system
C_{rx}	Communications receiver antennas number
C_{tx}	Communications transmitter antennas number
R_{rx}	Radar receiver antennas number
R_{tx}	Radar transmitter antennas number
$\mathbf{x}_{rad}(t)$	The transmitted radar signal
$x_{gui}(\theta)$	The transmitted-guided waveform
$\mathbf{y}_{rad}(t)$	The received radar signal
$\mathbf{y}_{jam}(t)$	Jamming signal
$\mathbf{y}_t(t)$	The target signal
θ_s	The target direction
β_s	The complex reflection coefficient
$\mathbf{y}_{gui}(\theta)$	The receive steering vector for the direction θ and $M_R \times 1$
K	sub-arrays notation
M_T	Transmitted sub-arrays
M_R	Received sub-arrays
s_k	The complex envelope of the signal
ϕ_k	The complex vector with a unit-norm that contains M_m beam-forming weights
w_k	The waveform vector of M_m orthogonal waveforms
M_m	The quantity of antenna elements presents in every sub-array
$\phi(t)_k^m$	The transmitted signal
$Q(t)$	The pulse shape
T_0	Duration time
$r(t,\theta)$	The reflected-off signal
$\beta(\theta)$	The coefficient of reflection, and is the. In addition,
$d_k^m(\theta)$	The vector of waveform diversity that is defined as $e^{-j\tau_k^m(\theta)}$
$\tau_k^m(\theta)$	The time of wave to travel from the first component to the next one
ε	The interfering signals number
$b(\theta)$	The vector of receive steering with size $M_R \times 1$ associated with angle θ
$\{e^{-j\tau_k^m(\theta)}\}_{m=1,k=1}^{M_m,K}$	The waveform diversity vector
$\mathbf{P}$	The projection channel matrix